

Optics Letters

Flexoelectro-optic liquid crystal analog phase-only modulator with a 2π range and 1 kHz switching

JULIAN A. J. FELLS,^{1,3}  XIUZE WANG,¹ STEVE J. ELSTON,¹ CHRIS WELCH,²  GEORG H. MEHL,² 
MARTIN J. BOOTH,¹ AND STEPHEN M. MORRIS^{1,4}

¹Department of Engineering Science, University of Oxford, Parks Road, Oxford OX1 3PJ, UK

²Department of Chemistry, University of Hull, Hull HU6 7RX, UK

³e-mail: julian.fells@eng.ox.ac.uk

⁴e-mail: stephen.morris@eng.ox.ac.uk

Received 2 July 2018; accepted 26 July 2018; posted 1 August 2018 (Doc. ID 336475); published 7 September 2018

We present a flexoelectro-optic liquid crystal (LC) analog phase modulator with $>2\pi$ phase range at a 1 kHz switching frequency. The chiral nematic LC mixture consists of the bimesogen CBC7CB with chiral dopant R5011, aligned in the uniform lying helix mode. The mixture exhibits $> \pm \pi/4$ rotation of the optic axis for a drive voltage of ± 21.5 V ($E = \pm 4.5$ V μm^{-1}). The rotation of the optic axis is converted into a phase modulation with the aid of a reflective device configuration incorporating a ~ 5 μm LC cell, a polarizer, two quarter-wave plates, and a mirror. The residual amplitude modulation is found to be $<23\%$. This flexoelectro-optic phase modulator combination has the potential to enable analog spatial light modulators with very fast frame rates suitable for a range of applications.

Published by The Optical Society under the terms of the [Creative Commons Attribution 4.0 License](#). Further distribution of this work must maintain attribution to the author(s) and the published article's title, journal citation, and DOI.

OCIS codes: (070.6120) Spatial light modulators; (230.3720) Liquid-crystal devices; (120.5060) Phase modulation; (050.5080) Phase shift; (110.1080) Active or adaptive optics.

<https://doi.org/10.1364/OL.43.004362>

Devices that allow an optical phase to be manipulated over a two-dimensional area have applications in holography [1], biomedical imaging [2], laser micromachining [3], free-space optical communication [4], and many other fields. Liquid crystal (LC) spatial light modulators (SLMs) are attractive components to perform this function because they can be relatively low in cost and offer high spatial resolution. SLMs are typically used in a reflective configuration, the reflector being divided up into an array of pixels, each one independently electrically controlled via a silicon backplane. For many applications, it is necessary to have full analog control over a 2π phase range for each pixel. Existing planar-aligned nematic LC SLMs are able to provide

multi-level phase modulation; however, they are restricted to frame rates below 100 Hz. An SLM that can simultaneously deliver 0 – 2π analog phase-only modulation and a fast frame rate would have the potential to enhance the performance of existing applications, as well as provide new opportunities.

Ferroelectric LC devices give much faster frame rates than nematic devices, but they have other unwanted side effects. Typically, they are bistable and, therefore, only suitable for binary phase modulation [5]. Alternatively, they can be driven in the deformed helix mode [6], but the helix deformation results in a large birefringence change, which would manifest as a large unwanted amplitude modulation. A chiral smectic ferroelectric LC device has shown a 1.96π phase range at 1 kHz but, with high nonlinearity, a steep transition with voltage and no information on amplitude modulation [7]. Recently, an anti-ferroelectric LC phase modulator was demonstrated to be capable of 2π phase modulation with <300 μs response time [8]. However, this required a thick device of the order of 50 μm . In practice, such a thick device would limit the minimum pixel pitch, restricting the spatial resolution achievable. LC phase modulators based on other LC mesophases such as the blue phase, as well as the uniform standing helix and uniform lying helix (ULH) in the chiral nematic LC phase have been investigated [9], but not found to fulfill all the desired specifications simultaneously.

LC phase modulators based on the flexoelectro-optic effect [10] in chiral nematic LCs in the ULH mode have been proposed previously and demonstrated to give a phase modulation range of 0.71π at 500 Hz and 0.52π at 1 kHz [11]. While fast, the low phase modulation range will be insufficient for many applications. The lack of a suitable technology for stable, fast, analog phase-only SLMs is a severe limitation for dynamic optical systems. In this Letter, we present a solution to this problem and demonstrate a new ULH device configuration which allows a full 2π analog phase modulation range, fast switching speeds, no unwanted residual amplitude modulation, and a thin device for good spatial resolution.

To enhance the phase modulation performance of flexoelectro-optic LC phase modulators, different optical configurations (I)–(III) have been investigated, shown in Fig. 1(a). The basic

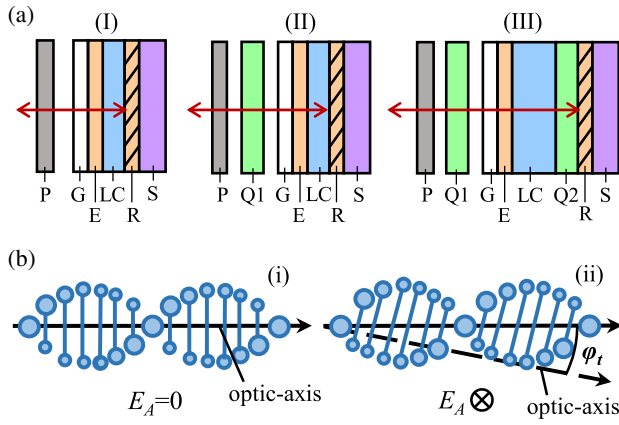


Fig. 1. (a) Three device configurations (I)–(III) of the optical phase modulator. P, polarizer; G, glass; E, transparent electrode; LC, liquid crystal; R, reflective electrode; S, silicon backplane; Q1, Q2, quarter-wave plates. The alignment layers on each side of the LC are omitted for clarity. The LC retardance is as follows: (I) $0.25\text{--}0.5\lambda$, (II) 0.25λ , and (III) 0.5λ . (b) Illustration of the flexoelectric-optic effect (i) under no applied electric field and (ii) with an electric field applied into the page.

configuration (I) has a ULH LC layer in a reflective configuration. This is similar to that employed by Chen *et al.* [11], but with an additional polarizer at the front to preserve the polarization state. An electric field is applied independently to each pixel between the reflective electrode (driven by the silicon backplane) and the transparent electrode on the inside surface of the glass cover. Rather than make the rear electrode reflective, it is also possible to use a dielectric mirror in front of it. Configuration (II) is similar to configuration (I), except that there is an additional quarter-wave plate after the polarizer, and the LC layer has a retardance of $\lambda/4$. Configuration (III) has, in addition, a second quarter-wave plate between the LC and the reflector and, in this case, the LC retardance is set to $\lambda/2$. This is similar to that of Stockley *et al.* [7]. Alternatively, a polymer cholesteric LC reflector may be used in place of the mirror and quarter-wave plate combination, which may be more manufacturable.

Figure 1(b) shows a diagrammatic illustration of the flexoelectric-optic effect. In the ULH mode, the LC forms a macroscopic helical structure, which is birefringent with an optic axis in a plane parallel to the substrates of the device. When an electric field is applied to the device, the coupling between the applied field and the field-induced flexoelectric polarization leads to a splay-bend distortion. This results in a macroscopic rotation (tilt) in the optic axis within the plane of the device. The LC may be modeled as a wave plate with an optic axis in a plane normal to the incident beam, whereby this angle changes with the amplitude of the applied field (and, hence, voltage). An expression for the output optical field, E_o , for configuration (III) is given by

$$E_o = PQ_1 \left(-\frac{\pi}{4} \right) D(-\varphi) Q_2 \left(-\frac{\pi}{4} \right) MQ_2 \left(\frac{\pi}{4} \right) D(\varphi) Q_1 \left(\frac{\pi}{4} \right) E_i, \quad (1)$$

where $D(\varphi)$ is the Jones matrix of an LC device having retardance δ at an orientation of angle φ to the horizontal [12], $Q_1(\frac{\pi}{4})$

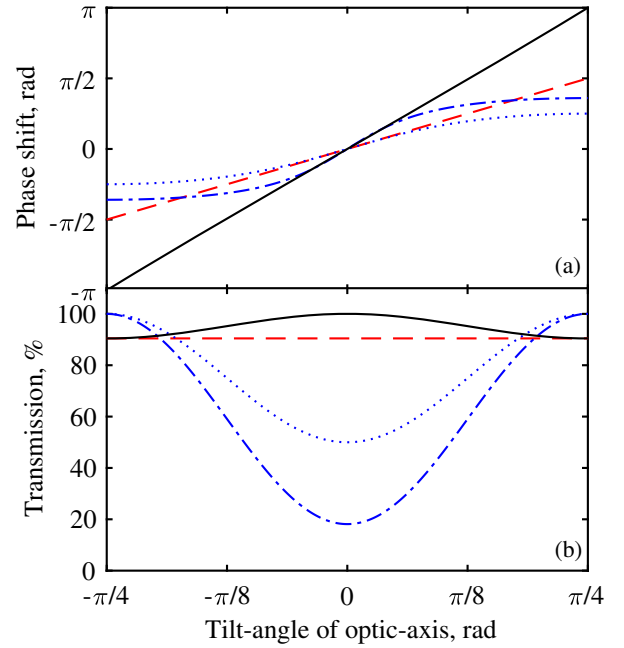


Fig. 2. Simulation of the optical phase modulator (a) phase shift and (b) transmission. (..... blue) configuration (I) with LC retardance 0.375λ ; (— · — blue) configuration (I) with LC retardance 0.32λ ; (--- red) configuration (II) with LC retardance 0.3λ ($\lambda/20$ error); (— black) configuration (III) with LC retardance 0.55λ ($\lambda/20$ error).

and $Q_2(\frac{\pi}{4})$ are the Jones Matrices for quarter-wave plates at $\pi/4$ to the horizontal, M is the Jones matrix of a mirror, E_i is the Jones vector for horizontally polarized light, and P is a horizontally aligned polarizer. Configuration (II) has the same output field as Eq. (1), but with Q_2 omitted. Configuration (I) also has the same output field as Eq. (1), but with both Q_1 and Q_2 omitted and the angle φ is offset by $\pi/4$.

Figures 2(a) and 2(b) show the theoretical phase shift and transmission, respectively, for the three configurations (I)–(III) presented in Fig. 1, using Eq. (1). Configuration (I) has an LC thickness chosen to give a retardance between 0.25 and 0.5λ . (Values above this give degenerate results.) At the upper end of this range, it is found that there is very little phase change whereas, at the lower end, there is a large amplitude modulation, so there is clearly a trade-off. Figure 2 shows that for a retardance of 0.375λ , the phase modulation range is 0.5π , but with 50% amplitude variation over this range (..... blue). Reducing the retardance to 0.32λ increases the phase modulation to 0.72π (similar to Ref. [11]) but, at the same time, the amplitude modulation increases to 81.9% (— · — blue). The limit of phase modulation possible for configuration (I) is π for 0.25λ retardance. However, as this limit is approached, the phase exhibits a sharp step change, and the transmission tends to zero in the transition region.

Figure 2 shows for comparison results from configuration (II) with a retardance error chosen to be $\lambda/20$, in addition to the nominal LC retardance of $\lambda/4$. These results show a marked improvement in the device performance compared to (I) by giving a larger, linear phase change and no amplitude modulation (--- red). A tilt-angle variation of $\pm\pi/4$ results in a π phase range. As the phase change is linear over all angles, no pre-biasing of the optic axis is required. However,

the retardance error does introduce a small loss of 9.5%, but this loss does not change with the phase setting.

Figure 2 also shows results for configuration (III) with a chosen retardance error of $\lambda/20$ in addition to the nominal LC retardance of $\lambda/2$. Figure 2 shows that a full 2π phase modulation range is achievable with a flexoelectro-optic device capable of only $\pm\pi/4$ change in the tilt angle. In addition, the dependence of the phase on the tilt angle of the optic axis is linear. The chosen retardance error introduces a small amplitude modulation of 9.5%. Recently, chiral nematic LCs consisting of the bimesogen CBC7CB have been shown to exhibit tilt angles $> \pm\pi/4$ with switching speeds of ~ 1 kHz [13]. Therefore, using a chiral nematic LC mixture composed of bimesogen compounds in configuration (III) has the potential to enable a full 2π analog phase range at switching speeds of > 1 kHz. Furthermore, SLMs can potentially be fabricated using this combination, enabling markedly higher switching rates than are currently attainable.

A bench-top implementation of configuration (III) with a bimesogen-based chiral nematic LC was constructed, and its phase response was measured using a Michelson interferometer,

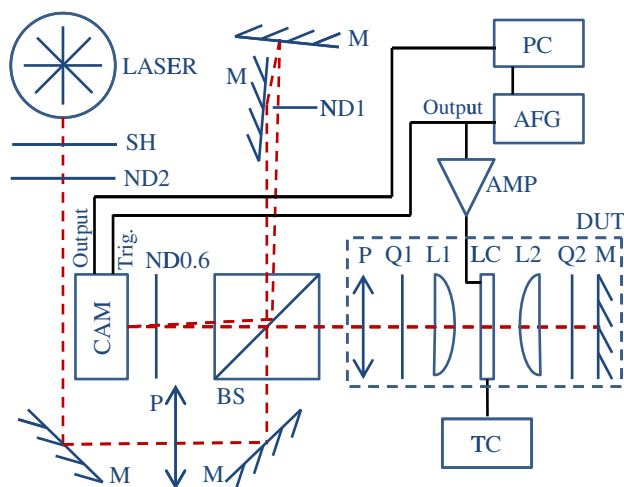


Fig. 3. Experimental arrangement to measure the phase of the proof-of-concept LC optical phase modulator: SH, shutter; ND x , neutral density filter of optical density x ; PC, personal computer; AFG, arbitrary function generator; AMP, amplifier; TC, temperature controller; CAM, camera; DUT, device under test; P, polarizer; Q1; Q2, quarter-wave plates; L1; L2, lenses; M, mirror; BS, non-polarizing beam splitter.

shown in Fig. 3. Light from a helium–neon laser at 632.8 nm (Uniphase 1125P) passes through a shutter, neutral density filter, and polarizer to a non-polarizing beam splitter (Newport 05BC16NP). One output port is directed to the reflective device under test (DUT). The other output port has two mirrors to reflect the light back with an angle offset to generate interference fringes at the CCD camera (Thorlabs DCU224C, 1280 \times 1024, 8-bit color). The interferometer was calibrated by using a nematic LC cell (E7) and mirror as the DUT to provide a known phase shift as a function of the applied electric field.

The LC DUT was then set up as per Fig. 3. The polarizer and quarter-wave plates were placed on rotation mounts. Q1 was then rotated to obtain right circular polarization, which was confirmed using a polarization analyzer (Schäfter + Kirchhoff SK010PA-VIS). Lenses L1 and L2 (respectively, Thorlabs LA1131A and LA1608) were used to focus the beam through the LC cell, which was mounted on a hot stage (Linkam LTS350 with TP93 controller). The LC was driven by a 1 kHz square-wave signal from an arbitrary function generator (AFG) (Wavetek 395) coupled to an amplifier (FLC Electronics F10AD). The camera was triggered from the AFG to record a 100 μ s exposure towards the end of each half-cycle of the square wave.

The LC mixture used consisted of the bimesogen CBC7CB dispersed with 3 wt. % R5011 (Merck Ltd.), which is a high twisting power chiral dopant. A nominally 5 μ m thick cell with antiparallel rubbed polyimide alignment layers and indium tin oxide electrodes was used. The thickness of the empty cell was measured to be 4.73 μ m from the Fabry–Perot fringes observed in the white-light transmission spectrum recorded on a UV-visible spectrometer (Agilent 8454). The cell was capillary filled with the LC mixture. The LC mixture exhibited a right-handed, chiral nematic phase between 102°C and 118°C. To align the cell in the ULH mode, the cell was heated above the clearing temperature of 118°C and allowed to cool in the presence of a 1 kHz ± 20 V signal applied to the cell. All subsequent measurements were carried out at 108°C. From Ref. [14], the extraordinary and ordinary refractive indices for CBC7CB at this temperature and a 633 nm wavelength are 1.69 and 1.555, respectively. Using an expression for the birefringence of the ULH structure [15], this translates into a retardance of 0.51λ . The pitch was estimated to be 245 nm by measuring the optical rotation with a polarizing microscope and using an expression in [16].

Figure 4 shows the interference fringes recorded on the camera in response to different applied peak voltage levels up to ± 21.5 V ($E = \pm 4.5$ V μ m $^{-1}$). It can be seen that the fringes

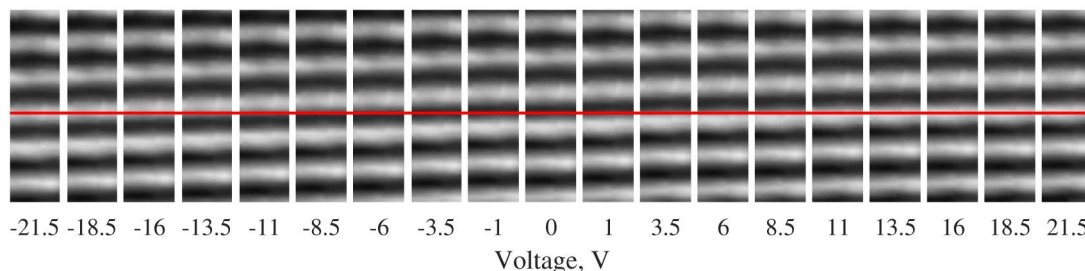


Fig. 4. Experimentally captured interference fringes for different voltages applied to the LC optical phase modulator. A 1 kHz amplitude signal was applied to the LC and the camera triggered on one half-cycle of the square wave to record the instantaneous fringe intensity pattern at each voltage level. The red line provides a reference phase.

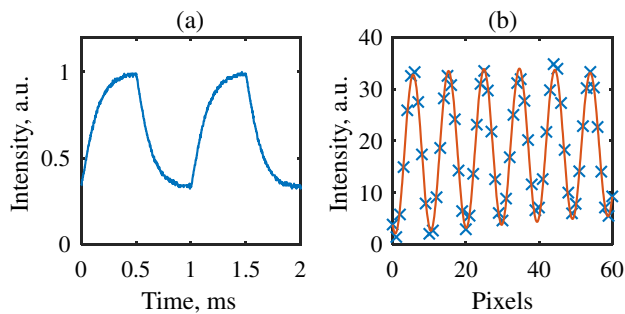


Fig. 5. Experimentally measured data: (a) optical transmission of LC through crossed polarizers (with no other components) under an applied 1 kHz square-wave drive of ± 11 V. The device optic axis at zero electric field was at an orientation of $\pi/8$ from the transmission axis of one of the polarizers. (b) (\times blue) fringe data recorded from the camera, (— red) fit to fringe data.

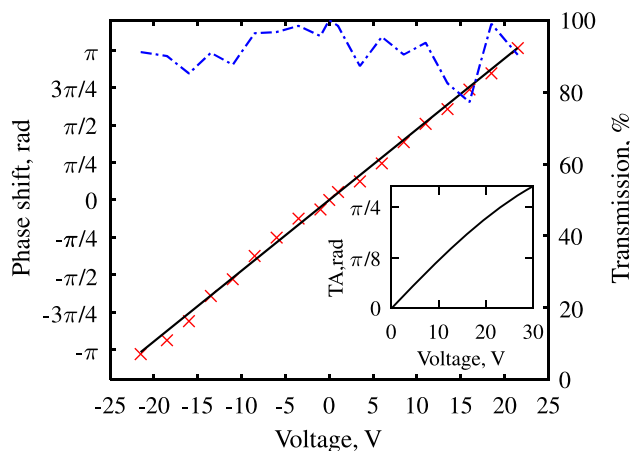


Fig. 6. Experimentally extracted phase (left axis) and transmission (right axis) for the LC optical phase modulator. (\times red) phase, (— blue) amplitude. Inset: tilt angle of the optic axis (TA) versus voltage for the LC mixture (without any additional components).

move relative to the reference line as the voltage is increased, all the way to the point that the next fringe reaches the line, demonstrating a 2π phase range. The 8-bit spatial data recorded from the camera were fitted to an interference pattern from two Gaussian beam profiles to determine the amplitude and relative phase at each voltage level. Figure 5(a) shows the optical transmission of the LC through crossed polarizers for an exemplar case of an applied 1 kHz square wave at ± 11 V. The change in the tilt angle at this drive voltage is approximately $\pm\pi/8$ rad, and it can be seen that the device permits 1 kHz switching. Figure 5(b) shows typical fitted data extracted from the fringe intensity data shown in Fig. 4.

Figure 6 shows the phase shift and amplitude variation for the bench-top phase modulator as a function of the applied voltage. The tilt angle and retardance were measured against

the voltage for the LC mixture, using a time-resolved technique described in Ref. [17]. The tilt angle of the optic axis is shown as an inset in Fig. 6, showing $> \pi/4$ angle change. The retardance was measured to vary between 0.51 and 0.54λ with voltage, which is within the chosen $\lambda/20$ tolerance for the simulation results. The phase range exceeds 2π and is approximately linear, as expected from Fig. 2. The amplitude variation is also low at less than 23%. However, this variation also includes noise from the experimental measurement system. It is possible that this amplitude fluctuation could be improved further by ensuring that the retardance is closer to a half-wave plate by adjusting the cell thickness and/or mixture composition.

In conclusion, we have demonstrated a new flexoelectro-optic LC phase modulator. The device uses a high tilt angle chiral nematic LC (CBC7CB with 3% R5011), a polarizer, two quarter-wave plates and a mirror. This configuration extends the reported modulation range of flexoelectro-optic phase modulators from 0.71π to $>2\pi$. The resulting LC optical phase modulator simultaneously achieves a full 0 – 2π analog phase range and a fast frame rate of 1 kHz, with low residual amplitude modulation of $<23\%$ in a thin ~ 5 μm device. We believe that the device presented in this Letter has the potential to be scaled up to a full high spatial resolution SLM using an LC-on-silicon fabrication process.

The research materials supporting this paper may be accessed in Dataset 1, Ref. [18].

Funding. Engineering and Physical Sciences Research Council (EPSRC) (EP/M017923/1).

REFERENCES

1. A. Jesacher, C. Maurer, A. Schwaighofer, S. Bernet, and M. Ritsch-Marte, *Opt. Express* **16**, 2597 (2008).
2. T. J. Gould, D. Burke, J. Bewersdorf, and M. J. Booth, *Opt. Express* **20**, 20998 (2012).
3. A. Jesacher and M. J. Booth, *Opt. Express* **18**, 21090 (2010).
4. A. Gomez, K. Shi, C. Quintana, M. Sato, G. Faulkner, B. C. Thomsen, and D. O'Brien, *IEEE Photonics Technol. Lett.* **27**, 367 (2015).
5. Z. Zhang, Z. You, and D. Chu, *Light Sci. Appl.* **3**, 1 (2014).
6. M. Schadt, V. G. Chigrinov, D. I. Dergachev, and E. P. Poshidaev, *Liq. Cryst.* **8292**, 1171 (2006).
7. J. E. Stockley, G. D. Sharp, S. A. Serati, and K. M. Johnson, *Opt. Lett.* **20**, 2441 (1995).
8. Z. Feng and K. Ishikawa, *Opt. Lett.* **43**, 251 (2018).
9. R. M. Hyman, A. Lorenz, and T. D. Wilkinson, *Liq. Cryst.* **43**, 83 (2016).
10. J. S. Patel and R. B. Meyer, *Phys. Rev. Lett.* **58**, 1538 (1987).
11. J. Chen, S. M. Morris, T. D. Wilkinson, J. P. Freeman, and H. J. Coles, *Opt. Express* **17**, 7130 (2009).
12. J. J. Gil and B. Eusebio, *Optik (Stuttgart)* **76**, 67 (1987).
13. A. Varanytsia and L. Chien, *Sci. Rep.* **7**, 41333 (2017).
14. G. Babakhanova, Z. Parsouzi, S. Paladugu, H. Wang, Y. A. Nastishin, S. V. Shiyanovskii, S. Sprunt, and O. D. Lavrentovich, *Phys. Rev. E* **96**, 1 (2017).
15. B. I. Outram and S. J. Elston, *Europhys. Lett.* **99**, 37007 (2012).
16. H. de Vries, *Acta Crystallogr.* **4**, 219 (1951).
17. J. A. J. Fells, S. J. Elston, M. J. Booth, and S. M. Morris, *Opt. Express* **26**, 6126 (2018).
18. www.eng.ox.ac.uk/smp/repository.